Available online at www.sciencedirect.com
ScienceDirect
Journal of Power Sources 169 (2007) 65–70
JOURNAL OF POWER SOURCES
www.elsevier.com/locate/jpowsour

Short communication

Electrochemical quartz crystal microbalance study of the electrodeposition of Co, Pt and Pt–Co alloy☆

A.J. Martín[a], A.M. Chaparro[a,*], L. Daza[a,b]

[a] *CIEMAT, Avda. Complutense, 22, 28040 Madrid, Spain*
[b] *Instituto de Catálisis y Petroleoquímica (CSIC), C/Marie Curie 2, Campus Cantoblanco, 28049 Madrid, Spain*

Available online 30 January 2007

Abstract

The electrochemical deposition of Co, Pt and Pt–Co alloy are studied with the electrochemical quartz crystal microbalance (EQCM) on a gold substrate. Co is deposited from acidic sulphate bath containing boric acid. Different processes are identified in this bath. Electrodeposition of Co on Au substrate is observed at potentials above redox potential, underpotential deposition, most probably due to formation of a Co–Au alloy. At more cathodic potentials, below −0.5 V, metallic Co is formed. The film is completely dissolved at positive potentials during the anodic scan, probably mediated by $Co(OH)_2$. The electrodeposition of platinum from acidic $PtCl_6^{2-}$ bath occurs below the thermodynamic potential (0.74 V) with almost 100% efficiency. At potentials negative from 0.0 V the efficiency decreases due to parallel water reduction. The codeposition of Co and Pt is also studied in acidic bath. Here, the decrease of pH due to water reduction on Pt deposits gives rise to precipitation of $Co(OH)_2$, together with the deposition of metallic Pt and Co. The films contain as major component the Pt_3Co alloy.

Keywords: Electrodeposition; Pt_3Co; Pt; Co; Quartz crystal microbalance; Electrocatalyst; PEMFC; Fuel cells

1. Introduction

The electrodeposition of metal and alloys is a technique that may have special interest for the synthesis of electrocatalysts for proton exchange membrane fuel cells (PEMFC). It is low temperature and non-vacuum technique, easily applied on different scales, from micrometric to macroscopic areas [1]. It also allows for a good control of the amount of electrocatalyst, and can be used to deposit films or particles of metals, alloys and compounds. For particles deposition, it is used the pulse deposition variant [2–6]. With respect to PEMFC catalysts, the principal electrocatalyst used at present is platinum and its binary alloys, that may enhance the activity towards water reduction and favour tolerance to CO in the anode [7,8]. Two main issues of major importance for PEMFC deployment, are the durability and cost of the electrocatalyst [9]. The electrodes with standard performance (0.5 W cm^{-2}) require about 0.5 mg cm^{-2} of platinum, which contributes to fuel cell cost with about US$ 40 kW^{-1} (above 70% of stack cost) according to present platinum prize [10]. This charge would probably be increased in case of massive production of fuel cells, requiring a significant part of world-wide platinum resources.

Electrodeposition, due to its particularities, may help in the preparation of electrodes with higher stability, using lower platinum content, as well as the synthesis of alternative catalysts based on new platinum forms, like incorporated in polymer films [11–13], platinum alloys [14,15], or new non-platinum catalysts [16]. During electrodeposition of platinum on carbon, the growth of hemispheric particles take place by the transfer of electrons from the electrode substrate to dissolved Pt(IV) species. Particles will deposit preferentially on electrochemically more active sites, like graphene edges (steps) and kinks, or surface oxigenated groups of carbon (aldehydes, alcohols and ketones), giving rise to a strong interaction with the substrate and more stable particles.

In this work, the deposition of Pt, Co and co-deposition of both are studied with the electrochemical quartz crystal microbalance (EQCM). Pt–Co alloys have shown enhanced kinetics towards oxygen reduction [17], and acceptable stability [18,19] which is of interest for the synthesis of more efficient electrocatalyst with lower Pt content. Co may be alloyed with Pt by direct electrodeposition in acidic [20,21] and basic ammonia solution [22,23]. Solid solution alloys can be obtained with

☆ This paper was presented at the 2nd National Congress on Fuel Cells, CONAPPICE 2006, Madrid, Spain, 18–20 October 2006.

* Corresponding author. Fax: +34 91346 6037.
E-mail address: antonio.mchaparro@ciemat.es (A.M. Chaparro).

0378-7753/$ – see front matter © 2007 Elsevier B.V. All rights reserved.
doi:10.1016/j.jpowsour.2007.01.043

composition and structure depending on deposition potential [20,21], where cobalt deposits underpotentially due to the negative enthalpy of Pt–Co alloys. This study is, to our knowledge, the first study of electrodepositon of PtCo alloy with EQCM. The analysis of the reactions that participate in the process of deposition of films is carried out, using the EQCM technique [24]. Finally, the study will be completed with XRD and XPS data for a structural and compositional characterisation of the deposits.

2. Experimental

For electrodeposition of Pt and Pt–Co alloy, the electrolyte composition includes H_2PtCl_6 (Aldrich), $CoSO_4{\cdot}7H_2O$ (Panreac), H_3BO_3 (Panreac), H_2SO_4 (Panreac). The solutions were prepared with deionised water. The pH of solutions measured with electronic pH-meter (Crison) was adjusted with H_2SO_4 and NaOH.

A commercial electrochemical microbalance has been used (Maxtek), with Au substrate (5 MHz, AT cut). The microbalance sensor is attached to the wall of an electrochemical cell as working electrode, using a platinum wire as counter electrode and a Ag/AgCl saturated electrode (0.20 V versus NHE) as reference. All potentials are given against NHE. The potential is controlled with a potentiostat (Autolab, Eco Chemie). All measurements are carried out at room temperature.

For XPS characterisation, a Perkin-Elmer PHI 5400 spectrometer was used, with Mg Kα radiation ($h\nu = 1253.6$ eV), 300 W source strength, and 25 mm × 25 mm beam size, under 10^{-9} Torr pressure in the sample chamber. Detector was at 45° with respect to substrate surface. For analysis and determination of binding energies, the signals were fitted to a symmetric Gaussian–Lorentzian (0.8–0.2) sum function after subtracting the background by the Shirley method. Binding energies were adjusted by fixing de C1s signal from adventitious hydrocarbon to $E_B = 285$ eV.

Before measurements, the EQCM was calibrated for the determination of the proportionality constant (C) between the change of resonance frequency (Δf) and the deposited mass (Δm) [25]:

$$\Delta m = C\,\Delta f \tag{1}$$

The value obtained from electrodeposition of Cu from a $CuSO_4$ 0.1 M, H_2SO_4 0.5 M solution, was $C = 43$ ng Hz^{-1}.

For the analysis of the EQCM results, a function that we call the *equivalent function* [Eq] was calculated from the experimental current and frequency change:

$$[\mathrm{Eq}] = F\,\frac{\mathrm{d}m}{\mathrm{d}Q} \tag{2}$$

where F is the Faraday constant and $\mathrm{d}m/\mathrm{d}Q$ is obtained by differentiation of the mass change on the electrode ($\mathrm{d}m = C\,\mathrm{d}f$) respect to the electrochemical charge ($\mathrm{d}Q = I/(\mathrm{v}\,\mathrm{d}E$, where v is the sweep rate)) without sign. Curves of Δf vs. E and ΔQ vs. E are averaged to 3 points per 100 mV interval, and the plot of Δf vs. ΔQ is derived and multiplied by F and the calibration constant (C) to obtain the equivalent function (Eq. (2)). The equivalent function is positive for electrodeposition processes and negative for electrodissolution. Its value equals the electrochemical equivalent of a substance when it is being deposited with 100% efficiency, i.e. without any other parallel process on the surface of the electrode. If parallel electrochemical processes occur with lower electrochemical equivalent or no mass change, the equivalent function will show a value decrease below the electrochemical equivalent of the reaction considered. In fact, the equivalent function can be written:

$$[\mathrm{Eq}] = \sum \mathrm{eq_i}\,\nu_\mathrm{i} \tag{3}$$

where $\mathrm{eq_i}$ is the electrochemical equivalent of each process and ν_i is its efficiency. With parallel chemical processes with deposit of mass (electroless, precipitation, ...) the equivalent function will have higher value than given by Eq. (3).

3. Results and discussion

The electrodeposition processes of Co, Pt and codeposition of Co and Pt are studied with EQCM in Figs. 1–4. For each case, the electrochemical current, the frequency shift, and the equivalent function are shown as a function of applied voltage.

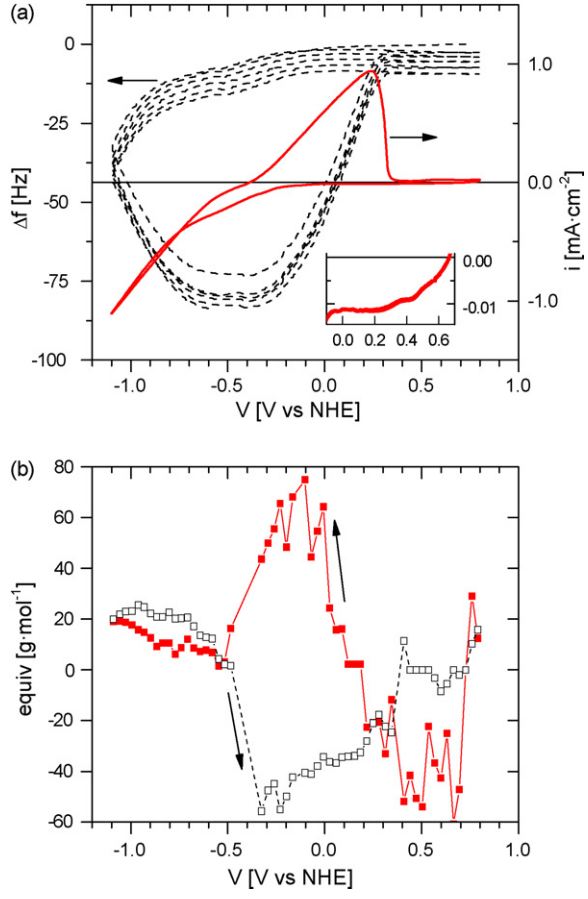

Fig. 1. (a) Current density and resonance frequency change for electrodeposition of Co on Au. (b) Equivalent function. Conditions are: H_3BO_3 (0.2 M) and $CoSO_4$ (10 mM) electrolyte; sweep rate: 50 mV s^{-1}; room temperature.

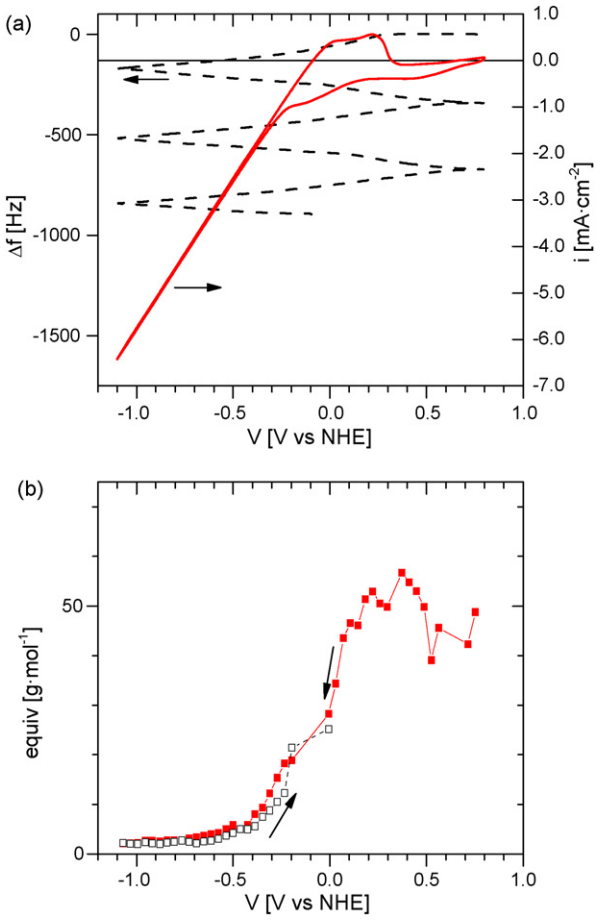

Fig. 2. (a) Current density and resonance frequency change for electrodeposition of Pt on Au. (b) Equivalent function. Conditions are: H_3BO_3 (0.2 M) and H_2PtCl_6 (1 mM) electrolyte; sweep rate 50 mV s^{-1}; room temperature.

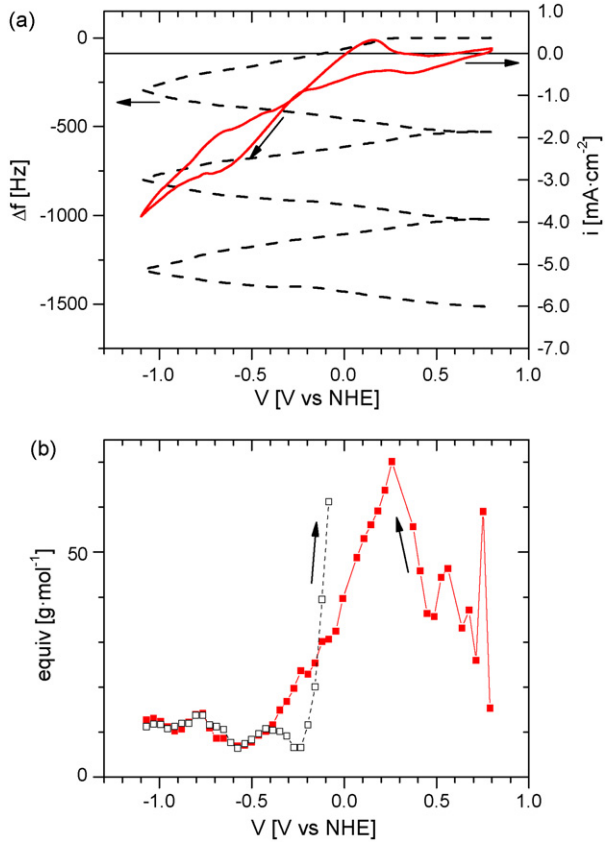

Fig. 3. (a) Current density and resonance frequency change for coelectrodeposition of Pt and Co on Au. (b) Equivalent function. Conditions: H_3BO_3 (0.2 M), H_2PtCl_6 (1 mM) and $CoSO_4$ (10 mM) electrolyte; sweep rate 50 mV s^{-1}; room temperature.

3.1. Cobalt electrodeposition

Starting with the cathodic scan, electrodeposition from a Co(II) solution is observed from 0.20 V (Fig. 1), when the equivalent function acquires a positive and constant value close to 60 g mol_e^{-1}. According to E^0 values (Table 1), this process cannot be attributed to electrodeposition of metallic Co^0 ($E^0 = -0.28$ V). The formation of an alloy with the substrate (Co–Au), leading to underpotential deposition of Co, is most probable [26]. Another possibility could be the electrochemical formation of cobalt(II) oxide (CoO) if residual oxygen remains in the solution (reaction (2), Table 1), however, measurements in O_2 saturated solution (not shown) show that current density in this potential range does not increase with respect to deaerated solutions, so underpotential deposition of Co is the most probable explanation. Previous to this process the reduction of Au oxides (see inset in Fig. 1a) might give rise to a negative value of the equivalent function. The function has not a clear value in this range, probably due to low current density and frequency changes, close to the noise level. Co^0 electrodeposition is thermodynamically possible at more negative potentials, below −0.34 V (reaction (5) in Table 1, $[Co^{2+}] = 10$ mM). Close to this potential a decrease in the equivalent function occurs, that we attribute to lower alloying efficiency. At more negative potentials, from −0.7 V, the equivalent function increases again to a value close to 30 g mol_e^{-1}, that can be attributed to metallic Co deposition. However, $Co(OH)_2$ precipitation at these negative potentials may also contribute, if a local pH increase occurs due to proton reduction.

Turning to the anodic scan, Co deposition continues until −0.5 V, when the equivalent function changes suddenly to a negative value in the range −60 to −30 g mol_e^{-1}. However, at this potential metallic cobalt is still thermodynamically stable, at least with respect to Co(II) formation (reaction (5)). One possibility is the dissolution of $Co(OH)_2$ upon increasing potential. Another possible explanation can be based on the oxidative formation of $Co(OH)_2$ (reaction (6)), followed by chemical

Table 1
Reactions involved in the electrodeposition of Pt and Co

No.	Reaction	E^0 (V)	Eq (g mol_e^{-1})
1	$Co(H_2O)_6^{3+} + e^- \leftrightarrow Co(H_2O)_6^{2+}$	+1.83	0
2	$Co^{2+} + 1/2O_2 + 2e^- \leftrightarrow CoO$	+0.83	37.5
3	$PtCl_6^{2-} + 4e^- \leftrightarrow Pt + 6Cl^-$	+0.74	48.8
4	$CoO + 2H^+ + 2e^- \leftrightarrow Co + H_2O$	−0.12	−4.0
5	$Co^{2+} + 2e^- \leftrightarrow Co$	−0.28	29.5
6	$Co(OH)_2 + 2e^- \leftrightarrow Co + 2OH^-$	−0.73	−17.0
7	$CoO + H_2O + 2e^- \leftrightarrow Co + 2OH^-$	−0.95	−8.0

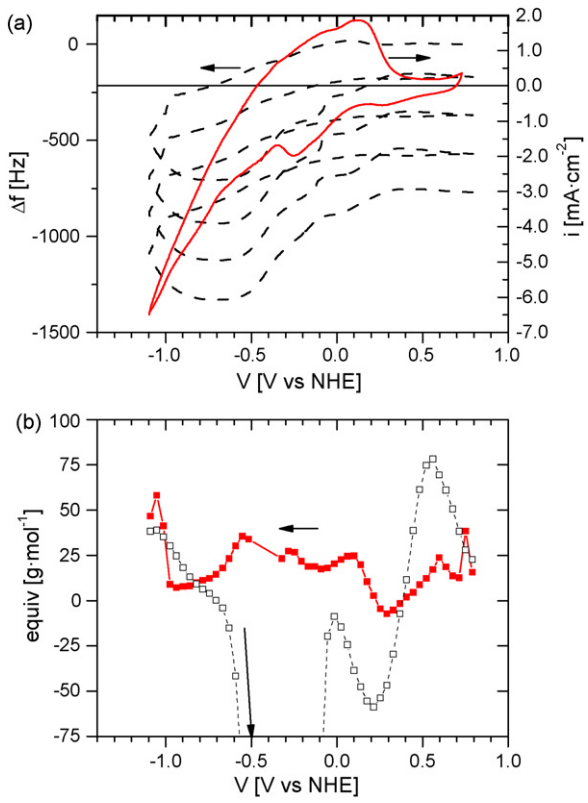

Fig. 4. (a) Current density and resonance frequency change for coelectrodeposition of Pt and Co on Au. (b) Equivalent function. Same conditions as in Fig. 3, except $CoSO_4$ (0.1 M).

dissolution. Such a mechanism has been proposed in basic, ammonia solution [27]. In the acidic solution, cobalt hydroxide may be readily dissolved after formation. A third possibility is the single electron oxidation of Co to Co(I) as the first step, which would explain an equivalent function value close to 60 g mol_e^{-1}, followed by the chemical reaction in solution close to the substrate surface from Co(I) to Co(II) and water reduction, like:

$$Co^{+} + H_2O \rightarrow Co^{2+} + OH^{-} + 0.5H_2 \quad (4)$$

Monoelectronic dissolution is observed for other divalent metals like Zn [28]. The final value of 30 g mol_e^{-1} at more anodic potential (0.0 to 0.2 V) indicates that Co is directly dissolved to Co(II). Finally, at more positive potentials (V > 0.2 V), the Co film is completely dissolved and frequency attains the starting value.

According to this EQCM analysis, the reaction sequence for Co electrodeposition and electrodissolution would be, for the cathodic scan:

$$Co^{2+} \rightarrow \text{Co underpotential} \rightarrow Co \quad (5)$$

and for the anodic:

$$Co \rightarrow [Co(I)] \rightarrow Co^{2+} \quad (6)$$

3.2. Platinum electrodeposition

Electrodeposition of platinum (Fig. 2) starts at 0.5 V, close to the thermodynamic potential ($E = 0.64$ V, for [Pt(IV)] = 1 mM, reaction (3) in Table 1), except for the first scan which is shifted to less positive potential (0.3 V). An overpotential for Pt electrodeposition on Au is expected, and has been attributed to the stability of the adsorbed $PtCl_6^{2-}$ complex [29], but once the electrodeposition of Pt is started, the overpotential is reduced. Equivalent function in Fig. 2b corresponds to the second scan. In the potential range from 0.5 to 0.1 V (cathodic scan), after platinum oxides have been reduced, the equivalent function attains a value close to the electrochemical equivalent for Pt(IV) (Table 1) which indicates the electrodeposition of Pt with efficiency close to 100%. Deposition current in this range has a constant value of 500 μA cm^{-2}, which may reflect a kinetically controlled electrodeposition [11]. At potentials negative from 0.1 V the value of the function decreases due to competing water reduction. Turning to positive-going scan the electrodeposition continues, and efficiency increases again when approaching 0 V.

3.3. Codeposition of cobalt and platinum

Codeposition of Co and Pt is studied in Figs. 3 and 4 at two concentrations of the Co salt. Under low Co(II) concentration, the features of the voltammetry are very similar to that of Fig. 2 for Pt deposition, except for a decrease in current value below −0.1 V, and a hysteresis at cathodic potentials. The equivalent function does not take a definite value, but oscillates in the range of 50 g mol_e^{-1} close to the equivalent of Pt and of the Pt–Co alloy according to reaction:

$$3PtCl_6^{2-} + CoSO_4 + 14e^{-} \leftrightarrow Pt_3Co + 18Cl^{-} + SO_4^{2-}$$

$$, \text{equiv} = 58.9\ \text{g mol}_e^{-1} \quad (7)$$

The function decreases at potentials below 0.2 V, due to competing water reduction, but shows some higher values in the cathodic limit, compare with platinum alone (Fig. 2b), that must be ascribed to the contribution of Co deposition, and probably some chemical precipitation of cobalt hydroxides due to local pH increase.

Increasing Co concentration introduces changes in the electrodeposition process (Fig. 4). From the frequency change, it is apparent that only a fraction, around 20%, of the

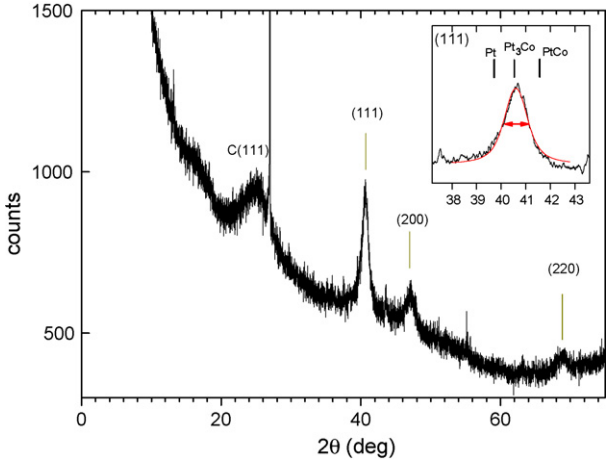

Fig. 5. XRD analysis of a Pt–Co alloy deposited under same conditions as electrode in Fig. 3, over carbon black surface. Inset, detail of (1 1 1) line.

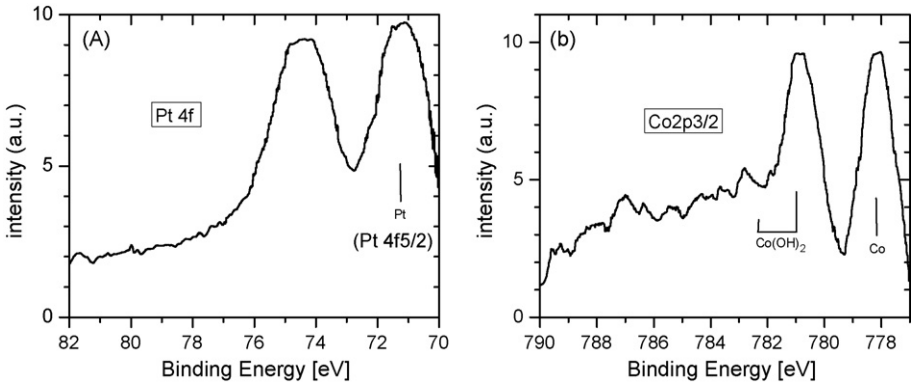

Fig. 6. XPS signal of Pt 4f (a) and Co 2p (b), corresponding to a Pt_3Co alloy electrodeposition under same conditions as electrode in Fig. 3.

electrodeposited film remains after a whole scan. The equivalent function attains a negative value during cathodic scan, $-7\,g\,mol_e^{-1}$ at 0.3 V, due to platinum oxides reduction ($PtO + 2H^+ + 2e^- \rightarrow Pt + H_2O$, equiv. $= -4\,g\,mol_e^{-1}$). It is positive at more negative potentials, close to $30\,g\,mol_e^{-1}$, reflecting the electrodeposition of cobalt and platinum. From −0.55 V the equivalent decreases, in the same way as for Co alone (Fig. 1), probably because water reduction reaction competes, and the final increase from −1.0 V to values close to $50\,g\,mol_e^{-1}$ that must be due to Pt and Co deposition, and probably some $Co(OH)_2$ precipitation.

The dissolution of a portion of the film in the anodic scan is evident from the high negative values of the equivalent function. This result indicates that the film is being dissolved both electrochemically and chemically, probably by dissolution of $Co(OH)_2$ precipitated at most negative potentials of the cathodic scan or after reaction (6). A high positive equivalent at 0.55 V must be due to the electrodeposition of oxides.

The analysis by XRD of codeposited Pt and Co films shows the formation of the Pt–Co alloy. According to JCPDS file 29-499, it may be ascribed to the alloy Pt_3Co (Fig. 5), although a continuous solid solution is reported in literature as a function of potential [18,19]. The XPS analysis shows that Pt (Fig. 6a) is predominantly in the metallic form, as inferred from binding energies of Pt 4f5/2 signal ($E_B = 71.2$ eV) [30]. As for Co (Fig. 6b) the signal corresponding to Co $2p_{3/2}$ shows two contributions, at $E_B = 778.3$ eV due to metallic Co^0, and at $E_B = 781.3$ eV due to $Co(OH)_2$, with 44 and 56% relative intensities, respectively. The presence of $Co(OH)_2$ in the films (an amorphous phase not detected by XRD) has been explained from the EQCM experiments, as a result of the electrochemically induced precipitation by water reduction.

4. Conclusions

Co, Pt and codeposition of both have been studied by means of the EQCM technique. Underpotential Co deposition to Co–Au alloy seems to occur. The electrodissolution of Co is complete at positive potentials and may take place by $Co(OH)_2$ intermediate or by means of single electron transfer reaction ($Co \rightarrow Co(I)$) followed, at more positive potential, by two electrons dissolution ($Co \rightarrow Co(II)$). Pt is observed to deposit almost from the thermodynamic potential with 100% efficiency, in the potential range positive from water reduction. Finally, Pt and Co codeposition gives rise to a film which partially dissolves at anodic potential. The remaining, stable film is analysed to be Pt–Co alloy (Pt_3Co).

Acknowledgements

This work has been financed by Comunidad de Madrid, program ENERCAM-CM, Ref. S-0505/ENE-304. Thanks are due to C. Maffiotte for XPS analysis.

References

[1] M. Paunovic, M. Schlesinger, Fundamentals of Electrochemical Deposition, Wiley, New York, 1998.
[2] M. Fleishmann, in: P. Delahay (Ed.), Advances in Electrochemistry and Electrochemical Engineering, vol. 3, Interscience Publishers, New York, 1963, p. 123.
[3] J.V. Zoval, J. Lee, S. Gorer, R.M. Penner, J. Phys. Chem. B 102 (1998) 1166–1175.
[4] A. Milchev, L. Heerman, Electrochim. Acta 48 (2003) 2903–2913.
[5] H. Natter, R. Hempelmann, Electrochim. Acta 49 (2003) 51–61.
[6] M. Hyde, R. Compton, J. Electroanal. Chem. 549 (2003) 1–12.
[7] P.N. Ross, in: J. Lipkowski, P.N. Ross (Eds.), Electrocatalysis, Wiley-VCH, Inc., 1998, p. 43.
[8] U.A. Paulus, A. Wokaun, G.G. Scherer, T.J. Schmidt, V. Stamenkovic, N.M. Markovic, P.N. Ross, Electrochim. Acta 47 (2002) 3787–3798.
[9] H.A. Gasteiger, S.S. Kocha, B. Sompalli, F.T. Wagner, Appl. Catal. B: Environ. 56 (2005) 9–35.
[10] Johnson Matthey Precious Metals Marketing, August 2006 Report, www.platinum.matthey.com.
[11] M. Hepel, J. Electrochem. Soc. 145 (1998) 124–134.
[12] K. Bouzek, K.-M. Mangold, K. Jüttner, Electrochim. Acta 46 (2000) 661–670.
[13] A.A. Mikhaylova, E.B. Molodkina, O.A. Khazova, V.S. Bagotzky, J. Electroanal. Chem. 509 (2001) 119–127.
[14] F.J. Rodríguez-Nieto, T.Y. Morante-Catacora, C.R. Cabrera, J. Electroanal. Chem. 571 (2004) 15–26.
[15] M.T. Giacomini, E.A. Ticianelli, J. McBreen, M. Balasubramanian, J. Electrochem. Soc. 148 (2001) A323–A329.
[16] B. Wang, J. Power Sources 152 (2005) 1–15.
[17] U.A. Paulus, A. Wokaun, G.G. Scherer, T.J. Schmidt, V. Stamenkovic, V. Radmilovic, N.M. Markovic, P.N. Ross, J. Phys. Chem. 106 (2002) 4181–4191.

[18] P. Yu, M. Pemberton, P. Plasse, J. Power Sources 144 (2005) 11–20.
[19] H.R. Colón-Mercado, B.N. Popov, J. Power Sources 155 (2006) 253–263.
[20] J.J. Mallett, E.B. Svedberg, S. Sayanc, A.J. Shapiro, L. Wielunski, T.E. Madey, P.J. Chen, W.F. Egelhoff Jr., T.P. Moffat, Electrochem. Solid-State Lett. 8 (2005) C15–C18.
[21] T.S. Eagleton, J. Mallet, X. Cheng, J. Wang, C.-L. Chien, P.C. Searson, J. Electrochem. Soc. 152 (2005) C27–C31.
[22] G. Pattanaik, G. Zangari, J. Electrochem. Soc. 153 (2006) C6–C10.
[23] F. Wang, K. Hosoiri, S. Doi, N. Okamoto, T. Kuzushima, T. Totsuka, T. Watanabe, Electrochem. Commun. 6 (2004) 1149–1152.
[24] K.K. Kanazawa, J.G. Gordon II, Anal. Chim. Acta 175 (1985) 99–105.
[25] G. Sauerbrey, Z. Phys. 155 (1959) 206.
[26] L. Cagnon, A. Gundel, T. Devolder, A. Morrone, C. Chappert, J.E. Schmidt, P. Allongue, Appl. Surf. Sci. 164 (2000) 24–28.
[27] D. Grujicic, B. Pesic, Electrochim. Acta 49 (2004) 4719–4732.
[28] R. Wiart, Electrochim. Acta 35 (1990) 1587.
[29] H.-F. Waibel, M. Kleinert, L.A. Kibler, D.M. Kolb, Electrochim. Acta 47 (2002) 1461–1467.
[30] D. Briggs, M.P. Seah, in: D. Briggs, M.P. Seah (Eds.), Practical Surface Analysis (Auger and X-Ray Photoelectron Spectroscopy, second ed., Wiley, Chichester, 1990.